JOURNAL OF SOLID STATE CHEMISTRY 100, 201–211 (1992)

Structural Characterization of R_2BaCuO_5 (R = Y, Lu, Yb, Tm, Er, Ho, Dy, Gd, Eu and Sm) Oxides by X-Ray and Neutron Diffraction

A. SALINAS-SANCHEZ,* J. L. GARCIA-MUÑOZ,†
J. RODRIGUEZ-CARVAJAL,† R. SAEZ-PUCHE,*
AND J. L. MARTINEZ†,‡

Departamento Química Inorgánica, Facultad de Ciencias Químicas. Universidad Complutense, Madrid E-28040, Madrid, Spain; and †Institut Laue-Langevin, B.P. 156-X, F-38042, Grenoble-Cedex, France

Received December 30, 1991; accepted March 3, 1992

R_2BaCuO_5 compounds with R = rare earth atom from Sm to Lu have been studied by neutron and X-ray powder diffraction. All of them are isostructural, and belong to the space group *Pnma* (Z = 4). A comparative study of the influence of the rare earth size on the structural parameters is presented. The stability of the structure is estimated from the agreement between valence bond sums and formal valence states. A systematic variation of the structural stability is found depending on the size of the rare earth atom. © 1992 Academic Press, Inc.

Introduction

The green-colored oxides R_2BaCuO_5 (R = Sm, Eu, Gd, Dy, Ho, Er, Tm, Yb, Lu, and Y) have been found very often as impurities in the synthesis of high-temperature superconducting $RBa_2Cu_3O_{7-x}$ oxides. These oxides, the so-called "green phases," are isostructural and their initial structural characterization was first reported by Michel and Raveau in 1982 (*1*) from powder X-ray diffraction studies. In this orthorhombic structure, with space group *Pnma* (Z = 4), the copper ions are situated in distorted square pyramids [CuO_5], connected by R_2O_{11} groups, which are formed from two monocapped trigonal prisms [R_7] sharing a triangular face; see Fig. 1. The Ba^{2+} is eleven-coordinated with oxygen, giving rise to very irregular polyhedra.

In 1986 Schiffler and Müller-Buschbaum (*2*) synthesized the first single-crystal of this family of oxides, Sm_2BaCuO_5, and from X-ray diffraction data confirmed the structural features previously reported by Michel and Raveau (*1*). In the last years, structure refinements of some R_2BaCuO_5 compounds have been published (*3–8*) from single-crystal X-ray and/or neutron powder diffraction studies.

Very recently, from magnetic susceptibility and heat capacity measurements, it has been shown that there exists an antiferromagnetic ordering at 30 K in the copper sublattice, which induces a subsequent ordering in the rare earth sublattice at lower temperatures for most of these oxides (*9–12*). In the present work we have analyzed in a compar-

‡ Present address: Instituto de Ciencia de Materiales de Madrid, Dep. Física Materiales (C-4), Universidad Autónoma de Madrid, Madrid, E-28049, Spain.

0022-4596/92 $5.00

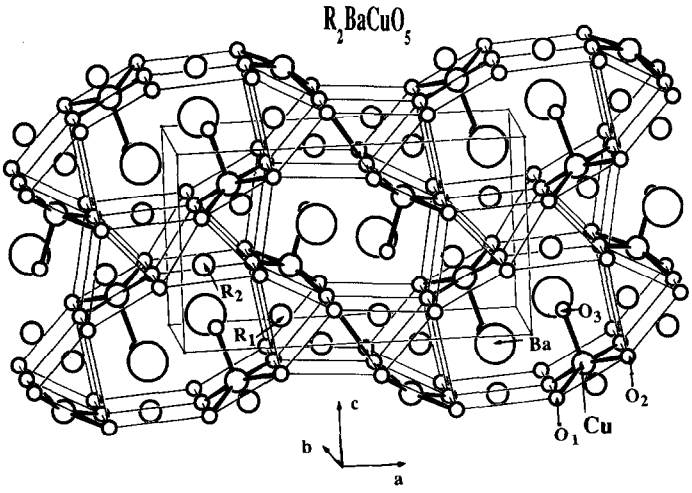

FIG. 1. Perspective view along the *b*-axis of the Sm_2BaCuO_5 structure type, showing the isolated square pyramids of $[CuO_5]$ and the trigonal prisms around the rare earth atoms.

ative way the structural features of these oxides, from X-ray and high-resolution neutron diffraction measurements. The relative stability of the different R_2BaCuO_5 oxides has also been studied using the bond valence method proposed by Brown (*13*).

The oxides with similar chemical composition but different transition metals (i.e., Cu, Ni, Co) are interesting because they are insulators and present different structural and magnetic properties. We initiate a systematic determination of the structural parameters for the different R_2BaMO_5 families. In this paper the structural aspect of the Cu family is emphasized. The goal is to determine the variation of the relevant geometrical parameters as a function of the rare earth ionic size. These parameters may have important consequences for their microscopic magnetic properties.

Experimental Details

R_2BaCuO_5 samples were prepared heating in air stoichiometric amounts of high purity oxides R_2O_3 (99.99%), CuO (99.999%), and $BaCO_3$ (A.R.) at 950°C for 48 hr, with two interruptions for grinding in order to homogenize the reaction products.

Neutron powder diffraction experiments were carried out in the High Flux Reactor of the Institut Laue-Langevin (Grenoble, France). In the present work we used the high-resolution powder diffractometer D2B (λ = 1.594 Å). This diffractometer is equipped with a bank of 64 detectors separated 2.5° in 2θ, spanning an angular range of 160°. Each detector is equipped with Soller slits. Scanning the detector bank by 2.5° in steps of 0.05°, one gets a full diffraction pattern. Most of the data were collected at room temperature (RT), otherwise the temperature is indicated. The high-resolution pattern, covering a wide angular range, permits the study of fine structural details. In particular, the oxygen positions can be determined with very high accuracy, in comparison with X-ray techniques.

X-ray powder patterns were recorded using a Siemens Kristalloflex 810 diffractometer and D-500 goniometer equipped with a secondary graphite monochromator and CuK_α radiation. The RT data were collected by step scanning over an angular range of

$10° < 2\theta < 120°$, in increments of 0.04° and a counting time of 15 sec per step.

All the data were analyzed with the Rietveld method using the program "FULLPROF" (*14*). The pseudo-Voigt profile function was used for describing the peak shape. No preferred crystallite orientation was taken into account. Refinement was done using the atomic positions in the *Pnma* ($Z = 4$) space group, and starting values for the free parameters taken from the literature.

Experimental Results

Neutron powder diffraction data were obtained at RT for R_2BaCuO_5 (R = Y, Ho, Er, Tm, Yb, and Lu). As an example, in Fig. 2a the pattern of Ho_2BaCuO_5 is shown. In the case of dysprosium oxide the neutron diffraction pattern, Fig. 2b, was only obtained at 50 K due to the availability of beam time. In order to avoid the high absorption cross section from dysprosium, a specially designed sample holder was used. For the remaining oxides of this series, i.e., R_2BaCuO_5 (R = Sm, Eu, Gd), where the absorption cross-sections are too high to use neutron diffraction techniques, we used X-ray powder diffraction. As an example the RT X-ray diffraction pattern of Eu_2BaCuO_5 is shown in Fig. 2c. The refinement was done using the starting values of positional parameters reported by Michel and Raveau (*1*) for the isostructural Y_2BaCuO_5 and Gd_2BaCuO_5 oxides. The lattice parameters and reliability factors for the different R_2BaCuO_5 compounds are given in Tables I and II. These parameters agree fairly well with those earlier reported by Wong-Ng *et al.* (*15*). The different diffraction data reveal that all the samples were single phase. As was expected, assuming the ionic model, the lattice parameters, a, b, and c of the unit cell decrease linearly as a function of the lanthanide ionic radius (*16*) in going from Sm^{3+} to Lu^{3+}. This has been represented in Fig. 3.

In Table III the final refined positional and thermal parameters for R_2BaCuO_5 (R = Y, Dy–Lu) are included. As was expected, the atomic coordinates obtained for each atom of the asymmetric unit are very close in all of these oxides. For the Y and Yb compounds our results agree very well with the previous single-crystal X-ray data (*5, 7*). It is worth noting that from high-resolution neutron powder diffraction it is possible to obtain a better accuracy in the location of oxygen atoms. Thus our data can be compared with those obtained by Pei *et al.* (*6*) and Lightfoot *et al.* (*8*) for Y, Yb, and Lu compounds.

The main interatomic distances are listed in Table IV. The careful analysis of the crystallographic data is very illustrative to better understand the structural effects of the ionic radius variation of the trivalent rare earth. This analysis allows a determination of the range of R^{3+}-ionic radii for which this structure-type is obtained. First, it can be observed that the size of the copper pyramid [CuO_5] remains almost constant for the different R_2BaCuO_5 oxides. This effect can be visualized in Fig. 4b, where the Cu–O(1), Cu–O(2), and Cu–O(3) distances have been plotted vs the radius of the different R^{3+} ions. The distances for the last three elements (Gd, Eu, and Sm) are not included because our X-ray powder data are not very precise in the determination of the oxygen positions. It is worth noting that although this structure type is also characteristic of R_2BaMO_5, where R is a small trivalent lanthanide cation and M = Ni, Zn, Co (*17–21*), the pyramid distortion is very different in each case. While, as can be observed in Table IV, the Cu–O(3) (apex) distance is about 11% larger than the other four, in the case of Ni, Zn, or Co isostructural compounds the M–O(3) distance is shorter than the mean M–O distances of the basal plane. On the other hand, this elongation of the [CuO_5] pyramid of the "green phases" is smaller than that reported for $Y_2Cu_2O_5$ (*22*).

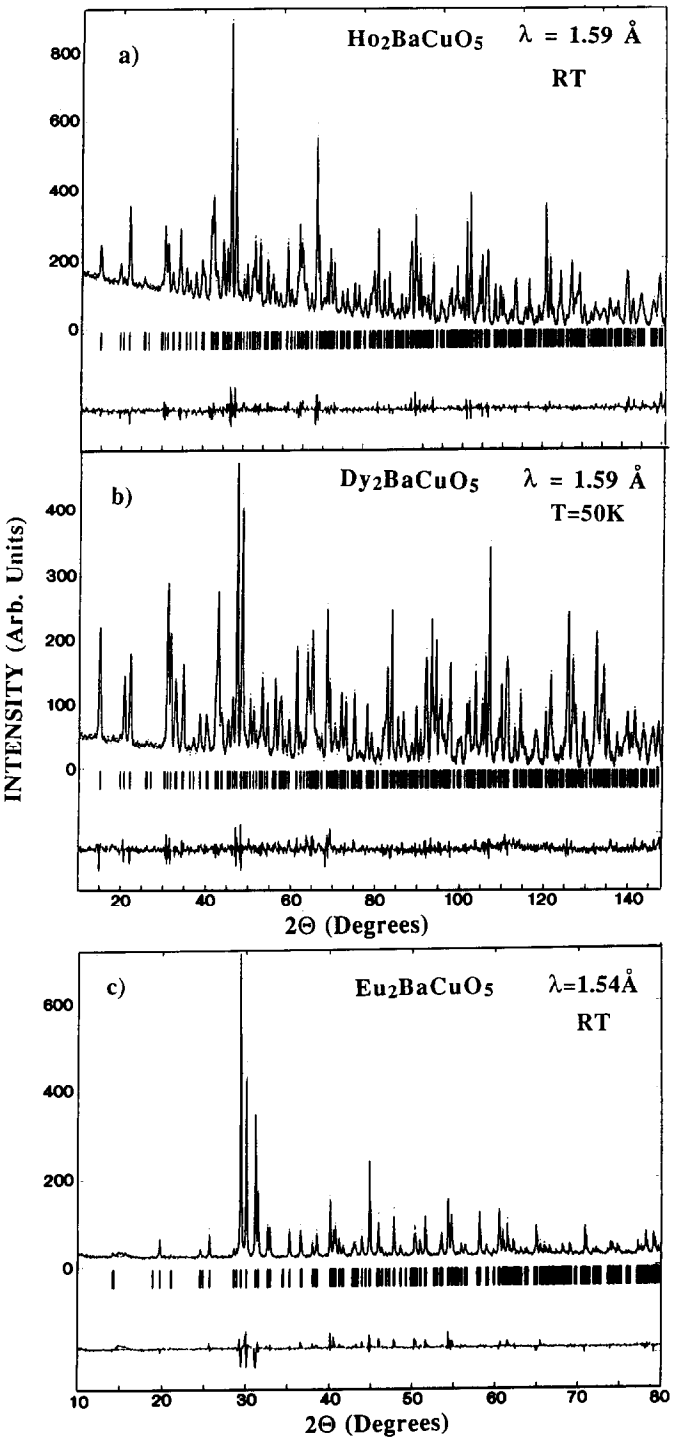

FIG. 2. Neutron (a and b) and X-ray (c) powder diffraction pattern (a) at RT for Ho_2BaCuO_5, (b) at 50 K for Dy_2BaCuO_5, and (c) at RT for Eu_2BaCuO_5. The solid line is the calculated profile; vertical marks show the position of allowed reflections. The difference curve is also plotted at the bottom part of each frame.

TABLE I

LATTICE PARAMETERS (Å) AND RELIABILITY FACTORS FOR R_2BaCuO_5 (R = Sm, Eu, Gd, AND Dy) FROM X-RAY POWDER DIFFRACTION DATA

	Sm_2BaCuO_5	Eu_2BaCuO_5	Gd_2BaCuO_5	Dy_2BaCuO_5
Lattice parameters (Å)				
a	12.4035(4)	12.3599(3)	12.3167(3)	12.2201(3)
b	5.7604(2)	5.7409(1)	5.7219(1)	5.6796(1)
c	7.2740(2)	7.2433(1)	7.2219(2)	7.1514(1)
Number of reflections				
	531	853	610	820
Reliability factors (%)				
R_{wp}	24.9	22.9	20.9	22.4
R_{exp}	19.2	13.6	14.8	10.5
χ^2	1.7	2.8	2.0	4.6
R_B	9.1	11.8	6.8	8.4

Note. Number of reflections included in the refinements are also shown.

In this latter case, the axial Cu–O is about 40% of the Cu–O basal plane distance. If we compare with the equivalent Ni family (i.e., R_2BaNiO_5), in this latter case the effect of the change of the rare earth is mostly observed in the NiO_6 octahedra (*23*). By contrast in the Cu family, the $[CuO_5]$ pyramids are not affected by the different size of the rare earth atoms.

Another important structural aspect concerns the angles $R(1)$–O(1)–$R(2)$ (Fig. 4a) and $R(2)$–O(2)–Cu (Fig. 4c), which can play an important role in the superexchange magnetic interactions. The variation with the ionic radius is very small for the former case. However, a systematic increase of 20 degrees/Å is observed for the latter.

Discussion

A systematic variation in the lattice parameters and cell volume is observed in the

TABLE II

LATTICE PARAMETERS (Å) AND RELIABILITY FACTORS FOR R_2BaCuO_5 (R = Dy, Ho, Y, Er, Tm, Yb, AND Lu) FROM HIGH-RESOLUTION POWDER DIFFRACTION DATA

	Dy_2BaCuO_5[a]	Ho_2BaCuO_5	Y_2BaCuO_5	Er_2BaCuO_5	Tm_2BaCuO_5	Yb_2BaCuO_5	Lu_2BaCuO_5
Lattice parameters							
a	12.2061(2)	12.1825(1)	12.1792(2)	12.1423(2)	12.1011(2)	12.0652(1)	12.0342(2)
b	5.6732(1)	5.6630(1)	5.6590(1)	5.6459(1)	5.6275(1)	5.6152(1)	5.6003(1)
c	7.1355(1)	7.1336(1)	7.1325(1)	7.1072(1)	7.0793(1)	7.0569(1)	7.0395(1)
Number of reflections	550	534	533	530	512	521	516
Fitted parameters	38	38	38	38	38	38	38
Reliability factor (%)							
R_{wp}	10.3	10.2	11.0	15.7	12.8	9.7	11.2
R_{exp}	7.5	5.1	8.2	13.7	10.0	5.5	8.1
χ^2	1.9	4.0	1.8	1.3	1.6	3.0	1.9
R_B	4.4	3.7	4.1	6.4	5.7	2.9	4.1

[a] Data at 50 K. Coherent scattering lengths (fm) are: $b_{Cu} = 7.718$, $b_O = 5.803$, $b_{Ba} = 5.25$, $b_{Dy} = 16.9$, $b_{Ho} = 8.08$, $b_Y = 7.75$, $b_{Er} = 8.03$, $b_{Tm} = 7.05$, $b_{Yb} = 12.40$, and $b_{Lu} = 7.3$.

TABLE III

REFINED ATOMIC COORDINATES AND ISOTROPIC TEMPERATURE FACTORS FOR R_2BaCuO_5 (R = Dy, Ho, Y, Er, Tm, Yb, AND Lu) OXIDES

		Dy_2BaCuO_5[a]	Ho_2BaCuO_5	Y_2BaCuO_5	Er_2BaCuO_5	Tm_2BaCuO_5	Yb_2BaCuO_5	Lu_2BaCuO_5
Ba	x	0.9049(4)	0.9048(3)	0.9049(2)	0.9057(4)	0.9045(3)	0.9048(3)	0.9039(3)
4(*c*)	y	1/4	1/4	1/4	1/4	1/4	1/4	1/4
	z	0.9291(7)	0.9304(5)	0.9307(4)	0.9307(7)	0.9298(5)	0.9292(5)	0.9306(4)
	B(Å^2)	0.56(9)	0.82(6)	0.81(5)	1.02(9)	0.84(7)	0.85(6)	0.69(6)
R(1)	x	0.2891(1)	0.2884(2)	0.2885(1)	0.2885(2)	0.28885(2)	0.2884(1)	0.2887(2)
4(*c*)	y	1/4	1/4	1/4	1/4	1/4	1/4	1/4
	z	0.1174(2)	0.1162(3)	0.1157(3)	0.1171(4)	0.1177(4)	0.1176(2)	0.1183(3)
	B(Å^2)	0.14(2)	0.32(3)	0.42(3)	0.52(4)	0.41(4)	0.42(2)	0.48(3)
R(2)	x	0.0744(2)	0.0740(2)	0.0738(2)	0.0743(3)	0.0738(2)	0.0738(1)	0.0736(2)
4(*c*)	y	1/4	1/4	1/4	1/4	1/4	1/4	1/4
	z	0.3969(2)	0.3957(2)	0.3960(2)	0.3965(4)	0.3969(3)	0.3972(2)	0.3967(3)
	B(Å^2)	0.05(2)	0.36(3)	0.49(3)	0.56(4)	0.44(4)	0.38(2)	0.57(3)
Cu	x	0.6599(3)	0.6595(2)	0.6589(2)	0.6599(3)	0.6597(2)	0.6594(2)	0.6594(2)
4(*c*)	y	1/4	1/4	1/4	1/4	1/4	1/4	1/4
	z	0.7114(4)	0.7130(3)	0.7132(3)	0.7123(4)	0.7120(3)	0.7126(3)	0.7130(3)
	B(Å^2)	0.12(5)	0.59(3)	0.49(3)	0.63(5)	0.42(4)	0.51(3)	0.47(3)
O(1)	x	0.4327(3)	0.4328(2)	0.4326(1)	0.4333(2)	0.4333(2)	0.4329(2)	0.4332(1)
8(*d*)	y	−0.0090(5)	−0.0073(4)	−0.0067(3)	−0.0076(6)	−0.0071(4)	−0.0065(4)	−0.0056(4)
	z	0.1674(3)	0.1660(2)	0.1661(2)	0.1661(3)	0.1644(2)	0.1649(2)	0.1638(2)
	B(Å^2)	0.27(5)	0.63(3)	0.56(2)	0.52(4)	0.43(3)	0.56(3)	0.49(3)
O(2)	x	0.2283(3)	0.2278(1)	0.2278(1)	0.2283(2)	0.2276(2)	0.2279(2)	0.2274(1)
8(*d*)	y	0.5042(7)	0.5040(5)	0.5045(4)	0.5024(7)	0.5014(5)	0.5025(4)	0.5015(4)
	z	0.3558(5)	0.3562(3)	0.3565(2)	0.3571(4)	0.3579(3)	0.3594(3)	0.3595(3)
	B(Å^2)	0.50(5)	0.84(3)	0.75(3)	0.79(4)	0.73(3)	0.71(3)	0.70(3)
O(3)	x	0.1003(3)	0.1004(2)	0.0997(2)	0.1008(3)	0.1010(2)	0.1011(2)	0.1011(2)
4(*c*)	y	1/4	1/4	1/4	1/4	1/4	1/4	1/4
	z	0.0820(6)	0.0806(4)	0.0802(4)	0.0832(6)	0.0830(5)	0.0847(5)	0.0850(4)
	B(Å^2)	0.13(7)	0.67(5)	0.47(4)	0.49(7)	0.32(5)	0.57(5)	0.43(5)

[a] At 50 K.

R_2BaCuO_5 family by changing the rare earth ion. However, until now we do not identify which parts of the structure are responsible for this behavior. The next step was to calculate the oxygen–oxygen distances inside each [CuO_5] pyramid. These are not usual distances to calculate, because the typical relevant parameters are the metal–oxygen distances. However, we already know that the distances Cu–O are very similar in all the compounds, but the underlying idea was to speculate that maybe the O–O distances were varying (i.e., the O–Cu–O angles) for different rare earth atoms. This is not the case either, as observed in Table V, where the oxygen–oxygen intrapyramid distances show nearly constant values. Now the next step was to evaluate the oxygen–oxygen distances between neighbor [CuO_5] pyramids (see Table V). This is an important distance to calculate if we take into account that the rare earth ions are placed between

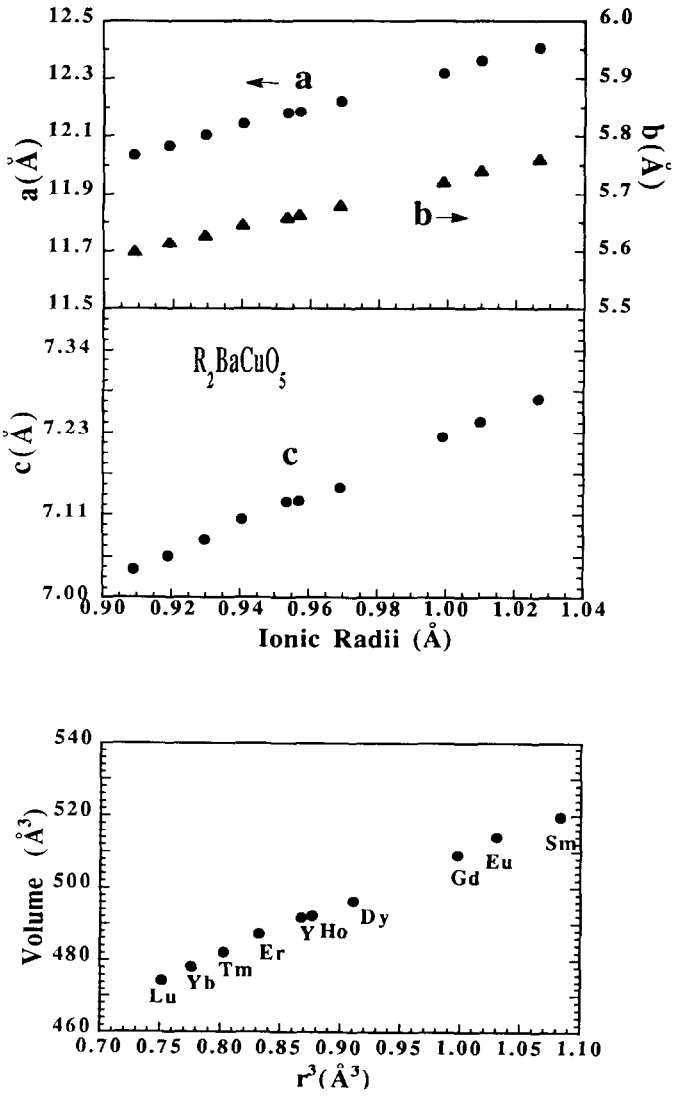

FIG. 3. Variation of the lattice parameters a, b, and c vs ionic radii for the different R_2BaCuO_5 oxides. The variation of the unit cell volume vs the third power of the ionic radii is also included in the lower frame.

different pyramids. The results are shown in Fig. 5. A similar linear dependence on the ionic radius, as is the case of the lattice parameters, is observed for the O(1)–O(1), O(1)–O(2), and O(2)–O(2) interpyramid distances. Finally, we identified which area of the structure was changing the most by the introduction of the different rare earth atoms.

In order to complete the study of the structural behavior of the R_2BaCuO_5 isomorphous compounds, we have applied the valence bond method to come to some conclusions about their overall structural be-

TABLE IV

MAIN INTERATOMIC DISTANCES (Å) FOR R_2BaCuO_5 (R = Dy, Ho, Y, Er, Tm, Yb, AND Lu) OXIDES

	Dy_2BaCuO_5[a]	Ho_2BaCuO_5	Y_2BaCuO_5	Er_2BaCuO_5	Tm_2BaCuO_5	Yb_2BaCuO_5	Lu_2BaCuO_5
Cu–O(1)(2×)	1.976(4)	1.974(3)	1.969(2)	1.975(4)	1.975(3)	1.964(3)	1.967(3)
–O(2)(2×)	2.012(5)	2.017(3)	2.020(3)	2.010(4)	2.015(3)	2.010(3)	2.013(3)
–O(3)(1×)	2.221(5)	2.215(4)	2.213(4)	2.219(5)	2.206(4)	2.213(4)	2.212(4)
R(1)–O(1)(2×)	2.318(4)	2.312(3)	2.306(2)	2.308(3)	2.296(3)	2.286(3)	2.275(3)
–O(2)(2×)	2.354(4)	2.355(3)	2.360(2)	2.340(4)	2.332(3)	2.336(3)	2.326(3)
–O(2)(2×)	2.344(4)	2.328(3)	2.321(3)	2.326(4)	2.319(3)	2.300(2)	2.301(3)
–O(3)(1×)	2.321(4)	2.304(3)	2.313(3)	2.292(4)	2.282(3)	2.272(3)	2.270(3)
R(2)–O(1)(2×)	2.371(3)	2.369(2)	2.369(2)	2.357(4)	2.337(3)	2.233(2)	2.327(2)
–O(1)(2×)	2.318(4)	2.297(3)	2.294(2)	2.290(4)	2.274(3)	2.271(3)	2.255(3)
–O(2)(2×)	2.389(4)	2.379(3)	2.382(3)	2.368(4)	2.354(3)	2.353(3)	2.341(3)
–O(3)(1×)	2.274(5)	2.271(3)	2.274(3)	2.250(5)	2.247(4)	2.230(3)	2.219(4)
Ba–O(1)(2×)	3.052(4)	3.060(4)	3.062(3)	3.038(5)	3.042(4)	3.030(4)	3.040(3)
–O(1)(2×)	3.257(5)	3.245(4)	3.240(3)	3.231(5)	3.235(4)	3.224(4)	3.213(3)
–O(2)(2×)	3.018(6)	3.006(4)	3.005(3)	2.991(5)	2.974(4)	2.965(4)	2.946(3)
–O(2)(2×)	2.958(6)	2.955(4)	2.956(3)	2.964(5)	2.943(4)	2.940(4)	2.933(3)
–O(3)(2×)	2.8416(2)	2.8333(2)	2.8311(1)	2.8258(3)	2.8160(2)	2.8102(2)	2.8030(2)
–O(3)(1×)	2.626(6)	2.613(4)	2.601(4)	2.605(6)	2.614(4)	2.610(4)	2.610(4)

[a] At 50 K.

TABLE V

MAIN OXYGEN–OXYGEN DISTANCES (Å) FOR R_2BaCuO_5 (R = Dy, Ho, Y, Er, Tm, Yb, AND Lu) OXIDES, INSIDE THE [CuO_5] PYRAMID AND BETWEEN NEIGHBORS [CuO_5] PYRAMIDS

		Dy_2BaCuO_5[a]	Ho_2BaCuO_5	Y_2BaCuO_5	Er_2BaCuO_5	Tm_2BaCuO_5	Yb_2BaCuO_5	Lu_2BaCuO_5
Intra	O(1)–O(1)	2.738(4)	2.914(2)	2.754(2)	2.737(5)	2.734(3)	2.735(3)	2.737(3)
Pyra-	O(1)–O(2)	2.838(5)	2.842(2)	2.840(2)	2.835(4)	2.841(3)	2.829(3)	2.834(2)
mid	O(2)–O(2)	2.792(6)	2.786(4)	2.779(3)	2.796(4)	2.798(4)	2.780(3)	2.783(3)
Inter	O(1)–O(1)	2.942(4)	2.914(3)	2.905(2)	2.909(5)	2.894(3)	2.881(3)	2.863(3)
Pyra-	O(1)–O(1)	2.907(4)	2.880(3)	2.884(2)	2.865(3)	2.834(3)	2.836(3)	2.812(2)
mid	O(1)–O(2)	2.974(5)	2.952(3)	2.949(2)	2.946(4)	2.916(3)	2.901(3)	2.885(2)
	O(2)–O(2)	2.888(6)	2.877(4)	2.880(3)	2.850(6)	2.830(4)	2.836(3)	2.817(3)

[a] At 50 K.

TABLE VI

VALENCE BOND SUMS (e.s.d's <0.01 v.u.) OBTAINED FOR THE DIFFERENT R_2BaCuO_5 (R = Dy, Ho, Y, Er, Tm, Yb, AND Lu) OXIDES

	Dy_2BaCuO_5	Ho_2BaCuO_5	Y_2BaCuO_5	Er_2BaCuO_5	Tm_2BaCuO_5	Yb_2BaCuO_5	Lu_2BaCuO_5
Ba	1.86	1.90	1.92	1.94	1.98	2.01	2.04
$R(1)$	3.11	3.08	3.01	3.03	3.03	2.98	2.91
$R(2)$	3.04	3.02	2.94	3.01	3.04	2.96	2.94
Cu	1.94	1.94	1.94	1.94	1.94	1.97	1.97

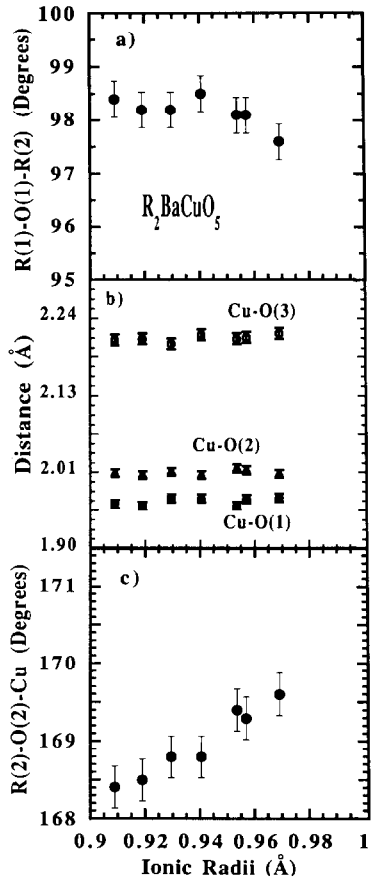

FIG. 4. (a) $R(1)$–O(1)–$R(2)$ exchange angle, (b) basal distances Cu–O(1) and Cu–O(2) and apex distance Cu–O(3) of the pyramid [CuO_5], and (c) $R(2)$–O(2)–Cu exchange angle vs the ionic radii for the different R_2BaCuO_5 oxides.

havior. The phenomenological relation between the bond length and the valence of a bond can be expressed as $s_{ij} = \exp[(R_0 - R_{ij})/B]$ (*13*), $B = 0.37$ being a "universal" constant and R_0 is a constant characteristic of the cation–anion pair. The valence sum rule (VSR) establishes that the sum of valence bonds around a cation (anion) must be equal to the formal valence (charge) of the i-cation (anion) (i.e., $\Sigma_j s_{ij} = V_i$). This method has been widely used by mineralogical crystallographers for many years, giving very useful results because the VSR is verified, within a few percent, for many inorganic compounds. However, one of the bases of the VSR is that the structure should permit the release of the stress introduced by the coexistence of different structural units, i.e., the structure should have enough degrees of freedom. In cases like *highly symmetric* structures or ions with *very strong* Jahn–Teller effect, or compounds with disorders or vacancies, such a simple calculation is of limited validity. The case of R_2BaCuO_5 oxides could be considered as belonging to the type of structures where the VSR should be fulfilled. All the calculations have been done at RT where the R_0 parameters are known (*24*) and diffraction data under similar conditions are available. From the deviation of the valence sum around each ion with respect to the expected value, there is a clear evidence of possible instabilities (or unusual features) in the crystal structure.

Table VI shows the valence bond sums for the different R_2BaCuO_5 oxides. The valence sums around barium increase with the decrease of the ionic size of the rare earth element. While for both crystallographic positions of the rare earth element, i.e., $R(1)$ and $R(2)$, a decrease is observed when the atomic number of R increases. As was expected for copper, the valence bond sums remain almost constant, which agrees with the data shown in Fig. 2b, where the Cu–O distances remain constant. Since the Cu^{2+} shows a Jahn–Teller effect the valence sums give a value of 1.94 valence units (v.u.) instead of the theoretical value of 2. However, for the last two compounds of the series (Yb and Lu) this value increases up to 1.97 v.u.

The root mean square of the bond valence sum deviations for all the atoms present in the asymmetric unit is a measure of the extend to which the VSR is violated over the whole structure (*25*). We shall call this value "global instability index (GII),"

$$\mathrm{GII} = \sqrt{\sum_{i=1}^{N} \left\{ \left(\sum_j s_{ij} - V_i \right)^2 \right\} \Big/ N}.$$

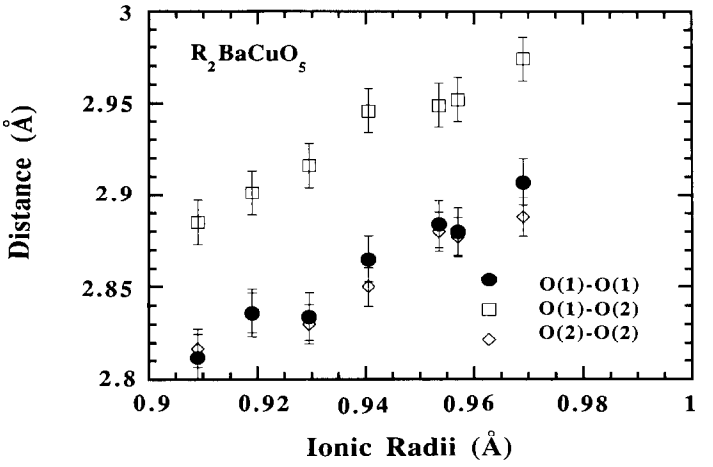

FIG. 5. Main oxygen–oxygen distances between neighbor [CuO_5] pyramids vs ionic radii.

In Fig. 6 we have plotted the variation of GII vs ionic radius for the family of R_2BaCuO_5 oxides. It can be observed that minimum values (higher stability) are obtained for the Er, Tm, and Yb oxides. When the ionic radius of the lanthanide cation increases, the instability index goes up taking its maximum value (less stable) for Sm_2BaCuO_5. This could justify the fact that for the Nd_2BaCuO_5 and $La_{1.8}Ba_{1.2}CuO_5$ oxides, having Nd^{3+} and La^{3+} with larger ionic radius than Sm^{3+}, this structure type does not exist. These two compounds adopt the Nd_2BaPtO_5-type structure, with tetragonal symmetry and space group $P4/nmb$ ($Z = 2$) (*26, 27*).

On the other hand, our experimental data show that for the smallest lanthanide cation, Lu^{3+}, the instability index starts to increase, which is indicative of larger stress in the

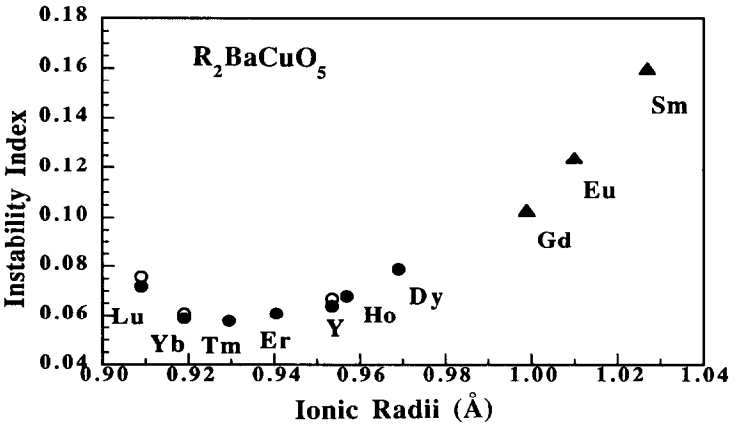

FIG. 6. Instability index of the different R_2BaCuO_5 compounds vs the ionic radii. The open circles are the data calculated from Refs. (*6*) and (*8*). The triangles are the data obtained from single-crystal X-ray diffraction study given in Refs. (*2*) and (*3*).

structure. Our attempts to prepare the hypothetical isostructural Sc_2BaCuO_5 oxide have been unsuccessful until now. The effect of decreasing the size of the ionic radius going from Lu^{3+} (0.91 Å) to Sc^{3+} (0.81 Å) should give higher values of the instability index parameter, which justify the nonexistence of the analogous compound of scandium with this structural type. As suggested by Brown (*25*) and Armbruster *et al.* (*28*), GII values higher than 0.2 v.u. indicate the presence of intrinsic strains large enough to cause instability at room temperature.

To conclude, we have shown in detail how the structure varies with the presence of different rare earth elements in this system. In particular, the $[CuO_5]$ pyramids remain unchanged, but the interpyramid distances vary as a function of the rare earth. The global instability index of the structure depends on the rare earth and probably presents a critical value above which this structure type does not exist. The shape of the GII vs ionic radius curve suggests the existence of an interval of allowed ionic radius for *R* atoms. The upper limit is around 1.05 Å, and the lower limit is below 0.9 Å.

References

1. C. Michel and B. Raveau, J. Solid State Chem. **43,** 73 (1982).
2. S. Schiffler and H. K. Müller-Buschbaum, *Z. Anorg. Allg. Chem.* **540/541,** 243 (1986).
3. J. A. Campa, J. M. Gomez de Salazar, E. Gutierrez Puebla, M. A. Monge, I. Rasines, and C. Ruiz Valero, *Phys. Rev. B* **37,** 529 (1988).
4. B. A. Hunter, S. L. Town, R. L. Davis, G. J. Russel, and K. N. R. Taylor, *Physica C* **161,** 594 (1989).
5. S. Sato and I. Nakada, *Acta Crystallogr., Sect. C* **45,** 523 (1989).
6. S. Pei, A. P. Paulikas, B. W. Veal, and J. D. Jorgensen, *Acta Crystallogr., Sect. C* **46,** 1986 (1990).
7. R. Norrestam, M. Hjorth, and J-O. Bovin, *Z. Kristallogr.* **183,** 245 (1988).
8. P. Lightfoot, S. Pei, J. D. Jorgensen, Y. C. Chang, P. Z. Jiang, and W. Veal, *J. Solid State Chem.* **89,** 385 (1990).
9. A. Salinas Sanchez, R. Saez Puche, and M. A. Alario Franco, *J. Solid State Chem.* **89,** 361 (1990). See also A. Salinas Sanchez, R. Saez Puche, and M. A. Alario Franco, *Eur. J. Solid State Inorg. Chem.* **T28,** 653 (1991).
10. R. Z. Levitin, B. V. Mill, V. V. Moshchalkov, N. A. Samarin, V. V. Snegirev, and J. Zoubkova, *J. Magn. Magn. Mater.* **90** and **91,** 536 (1990).
11. R. Burriel, M. Castro, C. Pique, A. Salinas Sanchez, and R. Saez Puche, *J. Magn. Magn. Mater.,* **104–107,** 619 (1992).
12. V. V. Moshchalkov, N. A. Samarin, I. O. Grishchenko, B. V. Mill, and J. Zoubkova, *Solid State Commun.* **78,** 879 (1991), and references therein.
13. I. D. Brown and D. Altermatt, *Acta Crystallogr., Sect. B* **41,** 244 (1985); **41,** 240 (1985).
14. J. Rodriguez-Carvajal, "FULLPROF: A Program for Rietveld Refinement and Pattern Matching Analysis," Abstracts of the Satellite Meeting on Powder Diffraction of the XV Congress of the International Union of Crystallography, p. 127, Toulouse France, 1990.
15. W. Wong-Ng, M. A. Kuchinski, H. F. McMurdie, and B. Paretzkin, *Powder Diffraction* **4,** 2 (1989).
16. R. D. Shannon and C. T. Prewitt, *Acta Crystallogr., Sect. B* **25,** 925 (1969).
17. H. Müller-Buschbaum and I. Ruter, *Z. Anorg. Allg. Chem.* **572,** 181 (1989).
18. A. Salinas Sanchez, R. Saez Puche, J. Rodriguez-Carvajal, and J. L. Martinez, *Solid State Commun.* **78,** 481 (1991).
19. H. Mevs and H. Müller-Buschbaum, *Z. Anorg. Allg. Chem.* **573,** 128 (1989).
20. H. Mevs and H. Müller-Buschbaum, *Z. Anorg. Allg. Chem.* **574,** 172 (1989).
21. C. Michel and B. Raveau, *J. Solid State Chem.* **49,** 150 (1983).
22. J. L. Garcia Muñoz, J. Rodriguez-Carvajal, X. Obradors, M. Vallet Regi, J. Gonzalez Calbet, and E. Garcia, *Phys. Lett. A* **149,** 319 (1990).
23. E. Garcia Matres, J. L. Martinez, J. Rodriguez-Carvajal, J. A. Alonso, A. Salinas Sanchez, and R. Saez Puche, submitted for publication.
24. N. E. Brese and M.O'Keeffe, *Acta Crystallogr., Sect. B* **47,** 192 (1991).
25. I. D. Brown, *Z. Krist.* **199,** 255 (1992).
26. C. Michel, L. Er-Rakho, and B. Raveau, *Rev. Chem. Miner.* **21,** 85 (1984).
27. T. Mochiku, H. Asano, F. Izumi, F. Mizuno, H. Masuda, I. Hirabayashi, and S. Tanaka, *J. Phys. Soc. Jpn.* **60,** 1959 (1991).
28. T. Armbruster, F. Röthlisberger, and F. Seifert, *Am. Miner.* **75,** 847 (1990).